

# A Model Treating Tensile Deformation of Semicrystalline Polymers: Quasi-Static Stress–Strain Relationship and Viscous Stress Determined for a Sample of Polyethylene

K. Hong, A. Rastogi, and G. Strobl\*

*Physikalisches Institut, Albert-Ludwigs-Universität, 79104 Freiburg, Germany*

*Received April 28, 2004; Revised Manuscript Received October 19, 2004*

**ABSTRACT:** Tensile deformation of semicrystalline polymers follows a common scheme with changes in the mechanism at critical strains. Choosing a poly(ethylene-co-12% vinyl acetate) (PEVA12) as an example, we measured true stress–strain relationships at constant strain rates, determined the elastic and plastic part of imposed strain in step-cycle experiments, and followed the stress relaxation at fixed strains. On the basis of the general observations, a model was constructed and then used for a description of the properties of PEVA12. The model treats the stress as arising from three contributions: quasi-static stresses originating from the stretched network of entangled chains in the fluid regions and from the force-transmitting skeleton of crystallites, plus the viscous forces described by Eyring's equation. Adjustment of the measured data to the model provides a decomposition of the stress in the three parts. With increasing strain the dominance shifts from the crystal- to network-transmitted stress, while the viscous forces increase continuously. Stress relaxation can be treated by an analytical solution of a differential equation that reproduces the results of the measurements.

## 1. Introduction

In previous work we studied the tensile deformation properties of several semicrystalline polymers. Experiments were carried out for linear, branched, and copolymerized polyethylenes,<sup>1</sup> poly-1-butene with copolymers,<sup>2</sup> syndiotactic polypropylene,<sup>3</sup> and poly( $\epsilon$ -caprolactone)<sup>4</sup> at ambient and for some of the systems also elevated temperatures.<sup>5</sup> Employing a video control in the stretching device, we always measured true stress–true strain dependencies for constant strain rates. Different from the engineering curves which can vary greatly due to the frequently occurring necking processes, these curves—which eliminate the necking effects—clearly demonstrate that tensile deformation of semicrystalline polymers follows a common scheme. Deformation mechanisms obviously change at four critical points which we denote A, B, C, and D. Most interestingly, the true strains at A, B, and C turn out to be invariant for each system; i.e., there is no change with the crystallinity which can be varied by the cunit content and with the temperature. Opposite to the strain, the stresses at the critical points vary, with larger values for higher crystallinities and lower values for higher temperatures. The observation indicates that the strain rather than the stress is essentially homogeneously distributed in the sample. Apparently, the crystallites in the sample can easily take up any imposed strain. This is possible because the crystalline lamellae possess a blocky substructure.<sup>6–8</sup> The blocks can slide against each other and by that take up the imposed strains. Block sliding sets in at point A at first as a local process and then turns, at point B, into a collective motion. The yield point in engineering stretching experiments is always located shortly above B. In consideration of the deformation properties a semicrystalline polymer can be viewed as a skeleton of crystallites, i.e., coupled blocks, intermingled with a network of entangled fluid chain sequences. At low stresses or strains the forces transmitted by the crystal skeleton

dominate, whereas at high strains the rubberlike network forces are superior. The network always exerts a stress on the crystallites. At point C this stress apparently reaches a critical value where blocks—oblique-oriented ones which experience the highest resolved shear stress—are no longer stable and become disassociated and transformed into fibrils. Point C, therefore, is associated with the onset of fibril formation. Polymer crystallization generally takes place without any disentangling processes; the entanglements existing in the melt are just shifted into the fluidlike regions. Cold stretched samples therefore often fully recover on a melting of the crystallites; the memory on the original shape of the sample is preserved by the entanglements of the network. This memory is only lost if the drawing goes to a state where disentangling starts. Exactly this is the property of point D. For strains above this point the entanglement structure changes, the memory gets lost and the sample does no longer fully recover on heating into the melt.

Our measurements of true stress–true strain relationships were always accompanied by recovery tests. By carrying out a stepwise stretching interrupted by unloading–loading cycles, it is possible to determine for each imposed strain which part is irreversible and which part recovers. It was found that the recoverable, elastic strain is always limited. It reaches a maximum value exactly at point C, the onset of fibrillation, and stays at this plateau value until point D, the onset of disentangling.

Stresses as observed in tensile stretching tests can be considered as being composed of three contributions: (i) the forces transmitted by the skeleton of crystal blocks, (ii) the force brought up by the stressed amorphous network, and (iii) viscous forces. Stress relaxation measurements at constant strain provide a means to determine the viscous forces. In a recent work such measurements were carried out for poly-1-butene.<sup>9</sup> Here, it was found that the amount of stress relaxation was always finite. The remaining quasi-stationary

stress can then be associated with the stress kept up by the crystal skeleton together with the network.

On the basis of the experimental observations, we now endeavored to construct a model. A model description should provide a decomposition of the measured stress into the contributions of the crystal skeleton, the amorphous network, and the viscosity; it should include a splitting of the total strain in an elastic and plastic part, should be able to describe the kinetics of stress relaxation at fixed strains, and should deal correctly with the effect of strain rate. This task should be accomplished with a minimum number of parameters. Physical knowledge is to be used as far as possible; however, a model of a complex process like the tensile drawing of a semicrystalline polymer will always also include empirical features. In the following we present such a model. It will be introduced with an example, the data obtained for a poly(ethylene-co-vinyl acetate). For this sample the viscous forces, the stresses transmitted by the crystal skeleton, and the stresses produced by the stretched amorphous network are of comparable magnitude. Furthermore, because this sample shows no necking, true stress–strain dependencies could be obtained without video control and therefore with a higher accuracy.

We shall present at first the experimental results and will then introduce the model, accompanied by some simple theoretical considerations. Then it will be shown how the model parameters can be derived from the experimental data. This paper is the first one of a series of publications dealing with experiments evaluated in the framework of the model. The next ones will discuss the change of Young's moduli during stretching, relations between creep and stress relaxation experiments, temperature dependencies of the model parameters, and their variation with the crystallinity, at first for polyethylenes and then also for other systems.

## 2. Experimental Section

The experiments were run using an Instron 4301 tensile testing device. Bone-shaped samples with a width of 4 mm were cut out of a 0.5 mm thick melt-crystallized film to carry out the experiments. As shown by the X-ray scattering patterns of stretched samples, the texture was always cylindrically symmetric; i.e., samples experienced a simple uniaxial drawing. All the tests were performed under computer control applying self-developed programs. Different experiments were carried out:

(i) Determinations of the relationship  $\sigma(\epsilon_H)$  between the true stress

$$\sigma = \frac{F}{A} = \frac{F}{A_0} \lambda \quad (1)$$

( $F$  = force,  $A$  = varying sample cross section,  $A_0$  = initial cross section,  $\lambda$  = extension ratio) and the true strain, also known as "Hencky strain"

$$\epsilon_H = \ln \lambda \quad (2)$$

for a fixed Hencky strain rate  $\dot{\epsilon}_H$  (we assume a constant volume).

(ii) Step-cycle tests: A stepwise stretching of the sample with a certain strain rate interrupted after each step with an unloading–loading cycle, yielding a splitting of the total true strain in a recoverable cyclic part and a nonrecovered "basic" part

$$\epsilon_H = \epsilon_{H,b} + \epsilon_{H,c} \quad (3)$$

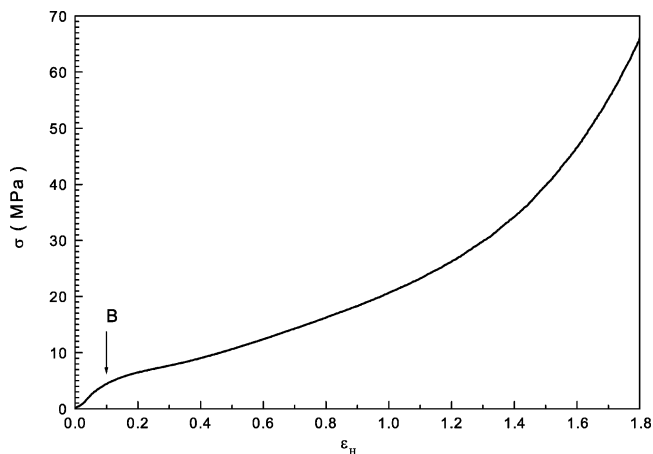


**Figure 1.** PEVA12: true stress–true strain dependence obtained for a strain rate  $\dot{\epsilon}_H = 0.005 \text{ s}^{-1}$ .

(iii) Stress relaxation measurements at fixed strains, yielding the time-dependent function

$$\Delta\sigma(t) = \sigma(0) - \sigma(t) \quad (4)$$

In addition, the device could also be used for creep measurements at fixed true stresses

$$\Delta\epsilon_H(t) = \epsilon_H(t) - \epsilon_H(0) \quad (5)$$

The stress relaxation and creep measurements were always carried out immediately after stretching the sample to some preset initial strain or stress.

The results presented in this work were obtained for a sample of polyethylene copolymerized with 12 wt % vinyl acetate units (PEVA12). As derived from DSC measurements, it had a crystallinity  $\phi_c = 0.33$ . The melting peak was located at 93 °C. We obtained this sample as a commercial product from Exxon Chemicals.

## 3. Results

**3.1. Stretching Curve and Step-Cycle Test.** Figure 1 shows the true stress–true strain dependence  $\sigma(\epsilon_H)$  of the sample selected for the studies (PEVA12) as obtained for a stretching with a Hencky strain rate of  $0.005 \text{ s}^{-1}$ . The shape of the curve indicates a strain softening which is later followed by a hardening. In the usually presented engineering stress–strain curves the yield point for necking samples is associated with a stress maximum and in nonnecking samples with the point on the curve where the curvature takes on the maximum value. In true stress–true strain curves of semicrystalline polymers a stress maximum does not occur—at least we did not find one in all the samples studied so far. An obvious choice for the yield point is here again the point with the maximum curvature, and we call it point B. For this sample we find, as indicated in Figure 1 stretching,  $\epsilon_H(B) \approx 0.1$ .

Figure 2 presents the result of a step-cycle test, again conducted with a strain rate of  $0.005 \text{ s}^{-1}$ . For a comparison also the result of the continuous stretching run is included. It is found to agree with the series of steps. Hence, the interruption by the cycles does not change the stretching properties. The strain recovered in the unloading down to zero stress gives the cyclic part, and the remaining strain represents the unrecovered basic part. The results of this decomposition carried out at various total strains are presented in Figure 3. The outcome includes a feature which is representative for all semicrystalline polymers: The cyclic part of the

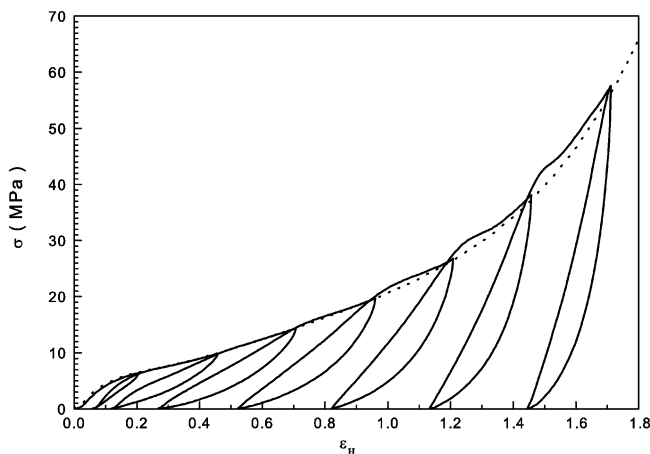


**Figure 2.** Step-cycle test carried out with a strain rate  $\dot{\epsilon}_H = 0.005 \text{ s}^{-1}$ . Comparison with the stretching curve of Figure 1 (broken line).

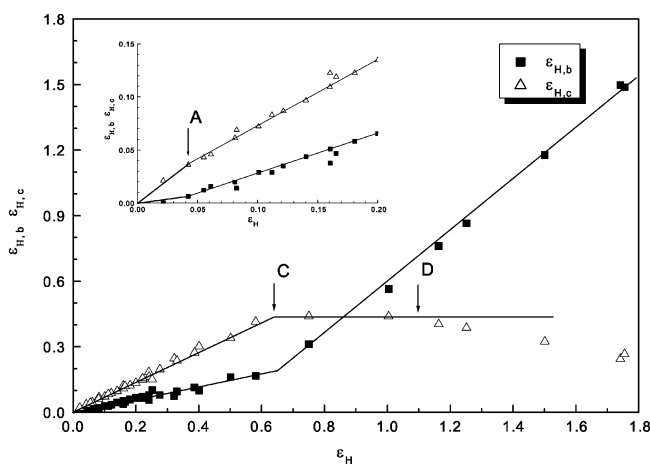


**Figure 3.** Cyclic and basic part of the total strain as derived from step cycle tests like the one shown in Figure 2.

strain shows a maximum value at a plateau. This is reached at  $\epsilon_H \approx 0.6$  and continues up to  $\epsilon_H \approx 1.1$ . As mentioned in the Introduction, the begin of the plateau defines the critical point C, the end the critical point D, and the two points are associated with the onset of fibrillation processes and of chain disentangling, respectively.

A nonrecovered part of the strain exists already below the yield point as is shown by the inset in Figure 3. In fact, plastic flow sets in already at the very begin of the stretching and shows a break at a strain  $\epsilon_H = 0.04$  where we allocate the critical point A. Note that point B does not show up in the curve. Hence, the strain softening observed at B is *not* due to the onset of flow, as the term yield point would suggest.

**3.2. Stress Relaxation Measurements.** Figure 4 presents some examples of stress relaxation measurements. Samples were stretched with four different strain rates to  $\epsilon_H = 0.4$ . There they were kept fixed, and the decay of the stress was registered. The initial stresses vary due to the different initial strain rates—the higher the strain rate, the higher they were—but as the curves show, finally all stresses become identical. There obviously exists a common relaxation curve, and only the starting points differ according to the initial strain rate.

A specific basic property of the curves becomes apparent in Figure 5, which shows the stress decay

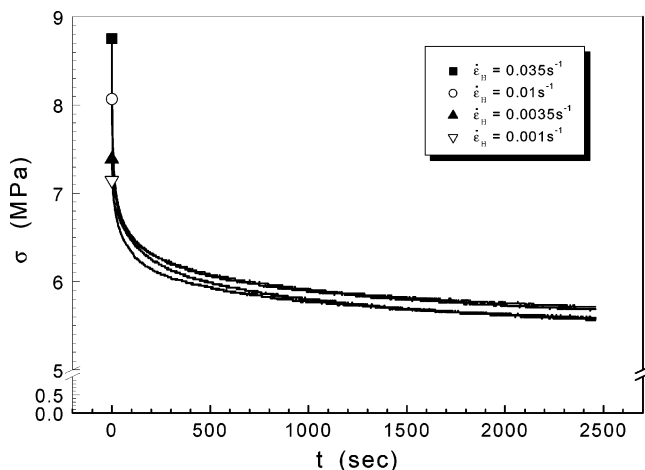


**Figure 4.** Stress relaxation after a stretching with the indicated strain rates to  $\epsilon_H = 0.4$ .

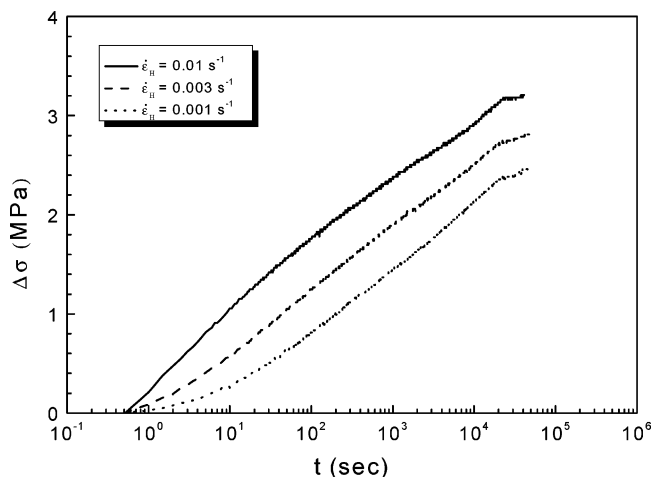


**Figure 5.** Stress relaxation  $\Delta\sigma(t) = \sigma(0) - \sigma(t)$  after a stretching with three different strain rates to  $\epsilon_H = 0.4$ . Long time experiments which indicate that after an extended period of a stress decay obeying a  $\log t$  law a final value is reached.

$$\Delta\sigma(t) = \sigma(0) - \sigma(t)$$

plotted vs  $\log t$  for some stress relaxation curves. One finds that the decay obeys over a large time range a logarithmic law,  $\Delta\sigma \sim \log t$ , and, in addition, that this range is finite. As it appears, a final value then is approached. Here this occurs after about  $10^4$  s. Such a behavior is found for all strains. Figure 6 gives the relaxation curve after stretching a sample to  $\epsilon_H = 0.8$ , again demonstrating the logarithmic time dependence after a certain initial period and the approach of a quasi-stationary state at the end. Figure 7 shows, in addition, some experiments that were less extended in time, obtained at intermediate fixed strains demonstrating again the validity of a logarithmic time law.

The information content of the stress relaxation measurements is obvious: The final magnitude of stress relaxation,  $\Delta\sigma(\epsilon_H, t \rightarrow \infty)$ , represents the contribution of viscous forces to the measured stress. Consequently, a subtraction of  $\Delta\sigma(\epsilon_H, \infty)$  from  $\sigma(\epsilon_H)$  yields the true stress—true strain relationship which would be obtained in the limit  $\dot{\epsilon}_H \rightarrow 0$  where all the viscous forces vanish. Figure 8 presents this “quasi-static” stress—strain dependence as derived from the stretching curve in Figure 1 and all conducted stress relaxation measurements. The open symbols represent an estimate of the quasi-static stress—strain relationship obtained by a

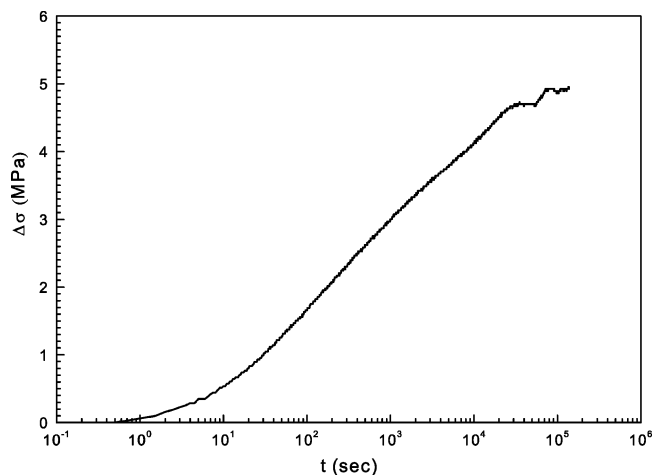


**Figure 6.** Stress relaxation after a stretching with  $\dot{\epsilon}_H = 0.001 \text{ s}^{-1}$  to  $\epsilon_H = 0.8$  followed over a long time until a quasi-stationary state is reached.

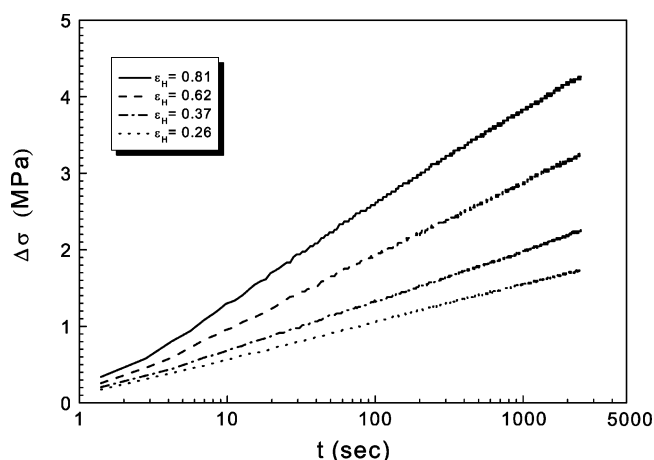


**Figure 7.** Stress relaxation  $\Delta\sigma(t)$  after a stretching with  $\dot{\epsilon}_H = 0.005 \text{ s}^{-1}$  to the given initial strains.

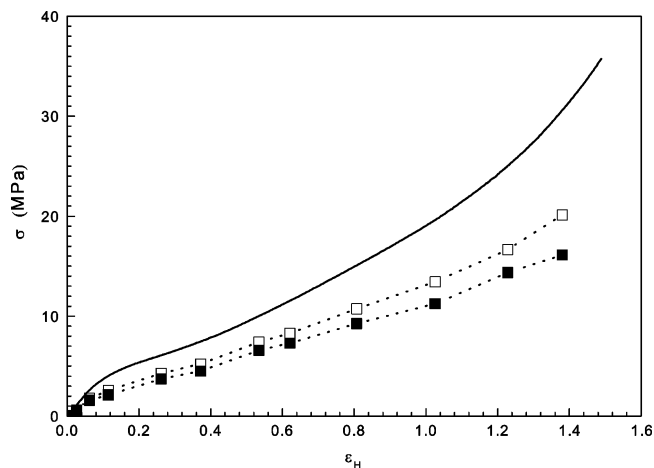


**Figure 8.** Stress-strain curve for  $\dot{\epsilon}_H = 0.005 \text{ s}^{-1}$ , stresses measured at various fixed strains after a relaxation time of 2500 s (open squares) and quasi-static stress-strain dependence as obtained by an extrapolation of the relaxation curves to infinite times (filled squares).

subtraction of the magnitude of stress decay after 2500 s. The filled symbols were obtained by an extrapolation of relaxation curves on the basis of a theoretical equation which will be introduced later.

Stress relaxation measurements can not only be carried out beginning at some point on the stretching

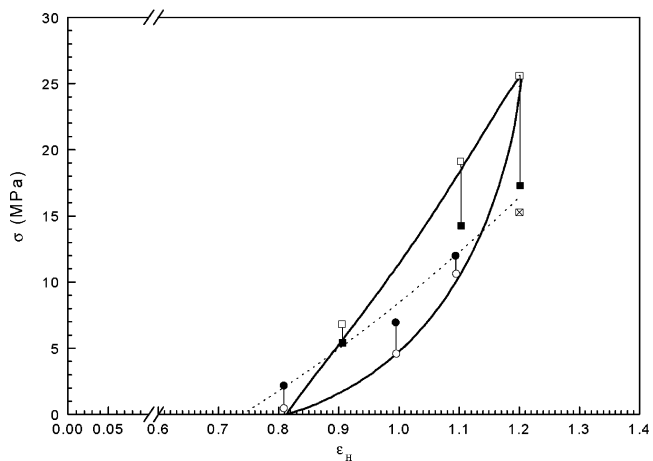
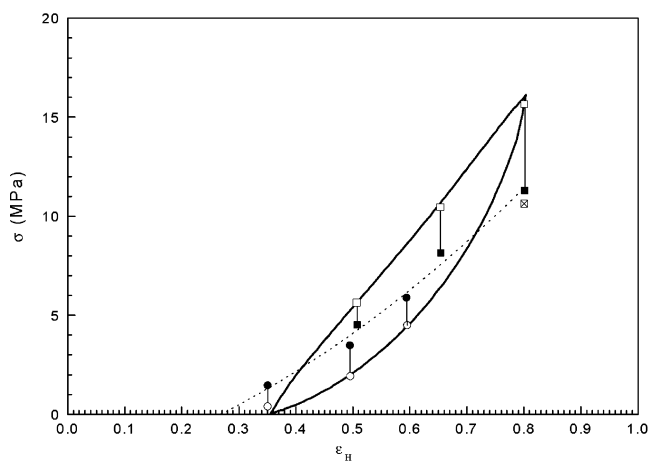
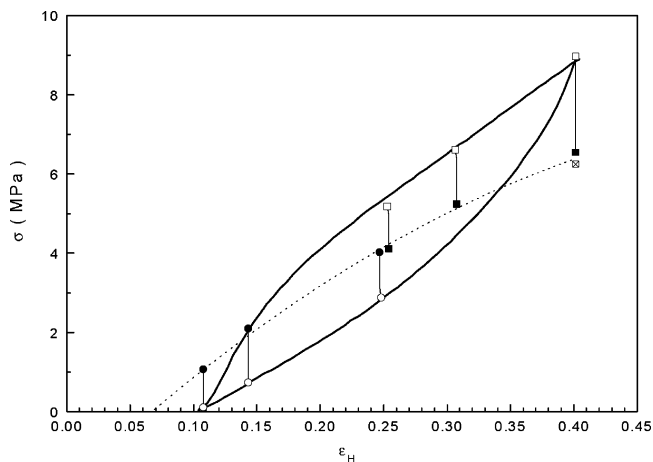


**Figure 9.** Cycles carried out with a strain rate  $\dot{\epsilon}_H = 0.005 \text{ s}^{-1}$  after a stretching to  $\epsilon_H = 0.4, 0.8,$  and  $1.2$ . The broken lines connect the relaxed stresses obtained at a series of points. They represent the respective purely elastic stress-strain relationships associated with the zero strain rate limit.

curve but also starting at any point on one of the cycles in the step-cycle tests. Figure 9 provides some examples. The filled symbols give the stresses which were measured after a constant relaxation time of 2500 s, where a quasi-stationary state was practically reached. Note that now stresses not always decrease but, during unloading, a stress can also increase. The broken line connects all the stresses reached after relaxations. It therefore shows again the behavior in the zero strain rate limit and thus represents the true elasticity non-affected by viscous forces of a sample drawn to a certain strain. Importantly, for  $\sigma = 0$  there remains also in the

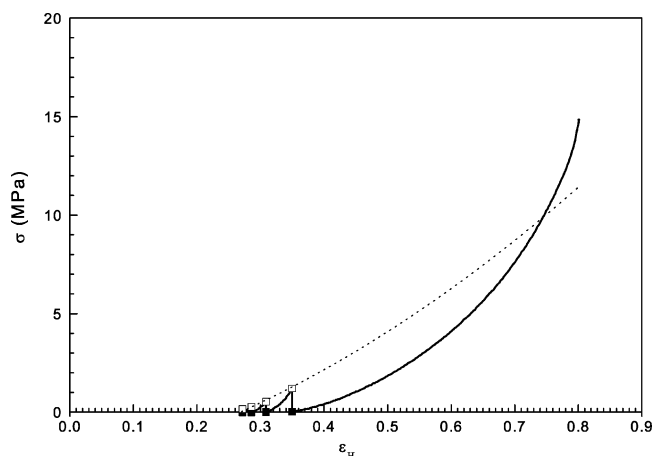


**Figure 10.** Determination of the plastic strain after a stretching to  $\epsilon_H = 0.8$ , achieved by repeated unloading steps after the repeated spontaneous stress increases. The broken line is identical with that shown in Figure 9, representing the elastic stress–strain relationship.

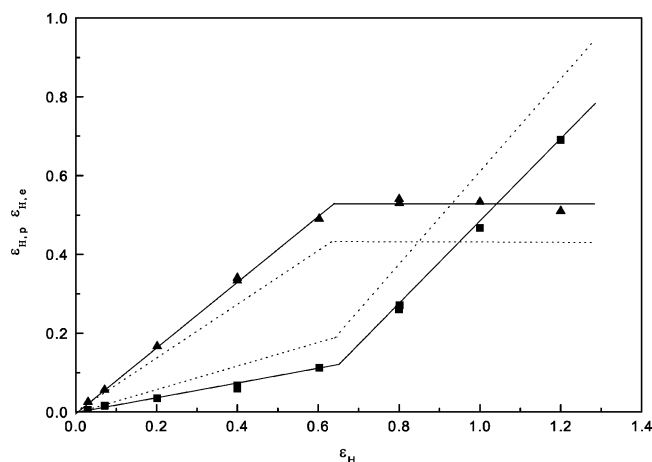


**Figure 11.** Plastic (squares) and elastic (triangles) parts of the total strain in the zero strain rate limit in a comparison with the basic and cyclic part derived from the step-cycle test in Figure 2 as given in Figure 3 (broken line).

quasi-static limit a finite strain which is a truly irreversible “plastic strain”. Figure 10 depicts a measurement which is focused on a determination of this plastic strain only: It shows a succession of unloading steps carried out after repeated spontaneous stress rises. As the figure shows, finally an equilibrium is reached. Figure 11 now presents the results of the decomposition of the total strain in the plastic and the elastic component, in a comparison with Figure 3, i.e., the decomposition following from a step-cycle test. The basic strain  $\epsilon_{H,b}$  is always somewhat larger than the final plastic strain  $\epsilon_{H,p}$  which would be found in the absence of viscous forces. However, the difference is not too large. As can also be noted the locations of the critical strains  $\epsilon_H(C)$  and  $\epsilon_H(D)$  are invariant.

#### 4. A Three-Component Model

There is a main finding in the relaxation measurements: Imposing a certain strain on a sample by stretching it with any chosen strain rate to that point and then letting the stress relax will finally lead into a quasi-stationary state. This is first indicated by the stress relaxation curves with a finite  $\log t$  range observed along the stretching curve and then shown clearly by the systematic stress increases and decays

defining together a limiting curve observed along the unloading and reloading parts of the cycles. This state is apparently well-defined, in two respects: (i) for a given imposed strain there results a certain final stress and vice versa, and (ii) the imposed strain has always an irreversible plastic part and a reversible elastic part

$$\epsilon_H = \epsilon_{H,p} + \epsilon_{H,e} \quad (6)$$

For the sample under study the two relations are depicted in Figures 8 and 11, respectively. With an increase of the imposed strain the quasi-stationary value of the stress increases as well. At first also both the plastic strain  $\epsilon_{H,p}$  and the elastic strain  $\epsilon_{H,e}$  increase, but then, at larger strains, the elastic strain reaches a maximum.

The stress measured in the quasi-stationary state arises—in the absence of viscous forces—from the two structural components in the sample, the network of entangled fluid sequences, and the skeleton of coupled crystal blocks. A stretched network produces a predictable force; the stress transmitted by the crystal skeleton, however, is of peculiar nature. In principle, a block sliding could lead to a complete decay of the force acting within the skeleton, but this is not observed. Therefore, the skeleton of blocks certainly does not resemble a purely viscous system. It cannot be treated like an ideal elasto-plastic body either. Such a system would remain purely elastic until a certain yield point, where a permanent flow at a constant stress would set in. The observations on semicrystalline polymers are different. There exists a plastic flow from the very beginning, down to smallest strains and stresses, and even more important, this flow is limited and remains finite at every imposed strain or applied stress. Hence, the crystal skeleton apparently shows a behavior which can be addressed as “finite plasticity”. This plasticity arises together with an elasticity which is rather high and finds its expression in the elastic strain  $\epsilon_{H,e}$ .

What could be the background of this behavior? Generally speaking, the plastic deformation remains finite because the sample hardens during the flow, in a manner, which finally brings the flow processes to an end. Indeed, a continuous hardening during plastic flow is a common assumption in constitutive equation theories dealing with the compression of amorphous polymers (see, e.g., ref 10) or in Andrade’s equation describing the creep of metals (compare, e.g., ref 11). Our suggestion, to introduce for semicrystalline polymers the notion of a quasi-stationary state with a permanent, nonvanishing stress which becomes established for each imposed strain after a sufficiently long time, goes a step further. In metals the hardening originates from stabilizing interactions between dislocations, whereas in semicrystalline polymers it is related to structural changes. These are partly reversible—those which accompany the unloading–reloading in the cycles—and partly quasi-permanent—those which remain at the end of the experiment shown in Figure 10. A comparison can also be drawn to a quite different field, namely ferromagnetism. Applying an external magnetic field  $H$  to an initially nonmagnetic sample produces a magnetization  $M$ . This happens from the beginning both, in irreversible manner by a shifting of Bloch walls, and reversibly, by a rotation of the magnetization within single Weiss domains. The analogy, with correspondences  $H/\sigma$  and  $M/\epsilon_H$ , is obvious; the Bloch wall movements correspond to the irreversible structure changes. Maybe

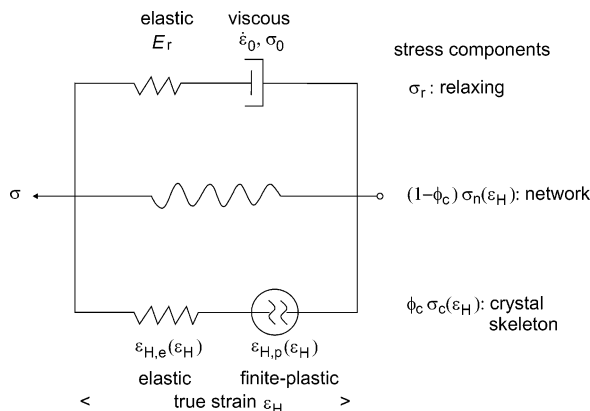


**Figure 12.** A three-component model treating the tensile deformation properties of semicrystalline polymers.

in the future a more microscopic understanding can be gained and a constitutive equation developed, but at present, one better accepts the behavior as being given and describes it by empirical means. Therefore, the novel step in the proposed treatment is presently just the assumption, suggested by the experiments, of the existence of a certain finite plasticity leading into a quasi-stationary state.

A comment can be given with regard to the plateau observed for the elasticity. For strains above  $\epsilon_H(C)$  a further elongation of the crystal skeleton is achieved by a morphological transition, namely the transformation of blocks into fibrils. This can indeed occur at a constant or only slowly increasing stress, in some sense comparable to a shear induced crystal–crystal transition.

A model constructed to treat tensile deformation of semicrystalline polymers must include the peculiar properties of the crystal skeleton as a core feature. The model which we propose is depicted in Figure 12, and the branch at the bottom deals with the stress  $\sigma_c$  transmitted by the crystal blocks. Corresponding to the elastic and plastic part of the deformation it is built up from two elements with properties as defined by the empirical relations  $\epsilon_{H,e}(\epsilon_H)$ ,  $\epsilon_{H,p}(\epsilon_H)$ , and  $\sigma_c(\epsilon_H)$ . The model includes, in addition to the crystal related branch, two more components. The second branch, drawn in the center, represents the stress  $\sigma_n$  arising from the network of entangled amorphous chains. We treat the network like an ideal rubber and thus characterize it by a certain shear modulus  $G$ . Different from polymer melts where the chain disentangling by reptative motions can lead to a stress decay in compressed samples (as treated, e.g., in a model by Bergstrom and Boyce<sup>12</sup>), entanglements cannot be removed in a strained semicrystalline polymer. The third, upper, relaxing stress branch relates to the stress  $\sigma_r$  which arises from the viscous forces in the sample. These forces show up when the sample is stretched with a finite strain rate  $\dot{\epsilon}_H$ . This component is meant to globally account for all the forces that originate from motions within both the crystalline and the amorphous parts of a semicrystalline sample.

That the three components are set to work in parallel manner is a choice suggested by the experimental observations. The existence of invariant critical strains rather than constant critical stresses speaks in favor of an essentially homogeneous strain in the sample. Indeed, this choice is not unusual looking at the setup of other models. In models dealing with the compression of amorphous polymers just above  $T_g$  developed by Boyce et al.<sup>10</sup> or Buckley and Jones<sup>13</sup> (viscous forces and

the network stress are also chosen to act in parallel fashion.

There is a further suggestion from the experiments, one which relates to the description of the viscous component in the relaxing stress branch. Stresses measured in stretching tests generally increase with a rising strain rate, but according to the relation

$$\sigma_r \sim \ln \dot{\epsilon}_H \quad (7)$$

rather than in the way of a Newtonian liquid

$$\sigma_r \sim \dot{\epsilon}_H \quad (8)$$

This suggests to describe the viscous force—as many other authors did (e.g., Argon,<sup>14</sup> Boyce et al.,<sup>10</sup> Tervoort and Govaert<sup>15,16</sup>)—by the Eyring law of viscosities

$$\frac{\sigma_r}{\sigma_0} = a \sinh \frac{\dot{\epsilon}_H}{\dot{\epsilon}_0} \quad (9)$$

In the limit  $\dot{\epsilon}_H \rightarrow 0$  the Eyring law becomes identical with the Newton law, with

$$\sigma_r \approx \frac{\sigma_0}{\dot{\epsilon}_0} \dot{\epsilon}_H \quad (10)$$

The Eyring law of viscosity uses two parameters: the reference stress  $\sigma_0$  and the reference strain rate  $\dot{\epsilon}_0$ , rather than one viscosity coefficient  $\eta_0$  only.  $\eta_0$ ,  $\sigma_0$ , and  $\dot{\epsilon}_0$  are related by

$$\frac{\sigma_0}{\dot{\epsilon}_0} = \eta_0 \quad (11)$$

We include in the relaxing stress part also an elastic element, with a Young's modulus  $E_r$ . In fact, with this choice it is possible to well reproduce the measured relaxation curves.

## 5. Adjustment of the Model to the Experiments

**5.1. Stress Relaxation Kinetics.** Stress relaxation, taking place at a constant imposed strain, affects in the proposed model only the upper branch. It is possible to treat this kinetics analytically and derive an explicit expression. Since we deal here with uniaxial extensions only, we can choose a simple scalar notation.

The total strain of the branch dealing with the relaxing stress is set up of two parts representing an elastic strain (modulus  $E_r$ ) and a viscous deformation (with Eyring parameters  $\sigma_0$  and  $\dot{\epsilon}_0$ ). We therefore write

$$\dot{\epsilon}_H = \frac{\dot{\sigma}_r}{E_r} + \dot{\epsilon}_0 \sinh\left(\frac{\sigma_r}{\sigma_0}\right) = 0 \quad (12)$$

or

$$\frac{d}{dt} \frac{\sigma_r}{\sigma_0} = -\frac{1}{\tau_r} \sinh\left(\frac{\sigma_r}{\sigma_0}\right) \quad (13)$$

with

$$\tau_r^{-1} = \frac{\dot{\epsilon}_0 E_r}{\sigma_0} = \frac{E_r}{\eta_0} \quad (14)$$

$\tau_r$  denotes the relaxation time which would be found in the Newtonian limit of very low stresses  $\sigma_r$ . This

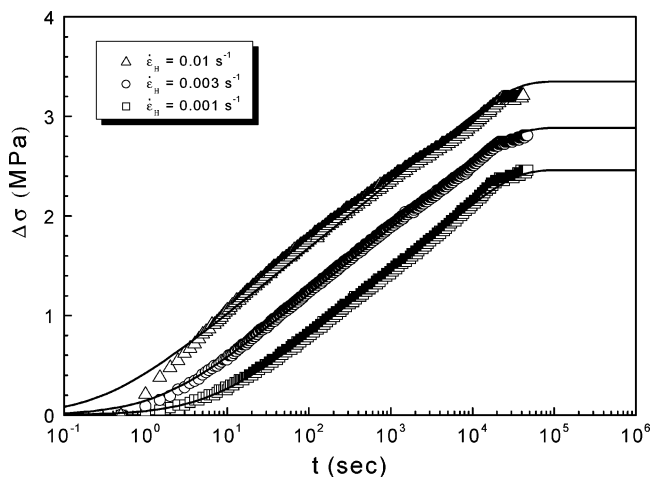


**Figure 13.** Stress relaxation curves from Figure 5 in comparison with model calculations ( $\tau_r = 1.6 \times 10^4$  s,  $\sigma_0 = 0.29$  MPa,  $\Delta\sigma_r(\infty) = 2.5, 2.9,$  and  $3.35$  MPa).

differential equation can be solved straightforwardly after a separation of the variables  $\sigma_r/\sigma_0$  and  $t/\tau_r$ . The result is

$$\frac{\sigma_r(t)}{\sigma_0} = 2 \operatorname{atanh} \left[ \tanh \left( \frac{\sigma_r(0)}{2\sigma_0} \right) \exp \left( -\frac{t}{\tau_r} \right) \right] \quad (15)$$

Using

$$\operatorname{atanh} x = \frac{1}{2} \ln \left( \frac{1+x}{1-x} \right) \quad (|x| < 1) \quad (16)$$

for times in the range

$$\frac{t}{\tau_r} \ll 1 \quad (17)$$

shows that eq 15 can be approximated by

$$\frac{\sigma_r(t)}{\sigma_0} \approx \ln \left( \frac{t}{\tau_r} \right) + \operatorname{const} \quad (18)$$

It is exactly this dependence which we have found experimentally, as is shown in Figures 5–7. The slopes in these figures, which are accurately determined, yield the value of the reference stress  $\sigma_0$ . The variation of the slopes indicates a variation of this parameter with the imposed strain. The experimental curve representing the stress decay  $\Delta\sigma$  is given in the model by

$$\Delta\sigma = \sigma(0) - \sigma(t) = \sigma_r(0) - \sigma_r(t) \quad (19)$$

$$\Delta\sigma = \sigma_r(0) - 2\sigma_0 \operatorname{atanh} \left[ \tanh \left( \frac{\sigma_r(0)}{2\sigma_0} \right) \exp \left( -\frac{t}{\tau_r} \right) \right] \quad (20)$$

Fitting the experimental data by this expression yields the three parameters  $\sigma_0$ ,  $\tau_r$ , and  $\sigma_r(0)$ . Such fits were carried out for various values of the imposed strain and are shown, referring to the curves previously presented in Figures 13–15. The data representation looks satisfactory; the values derived from the fits are always given in the corresponding legends. As a comparison of the fits in Figures 13 and 14 shows, there is no change in the relaxation time  $\tau_r$ ; results suggest to choose as a unique value for all strains,  $\tau_r = 1.6 \times 10^4$  s. The reference stress  $\sigma_0$  and the total amount of stress

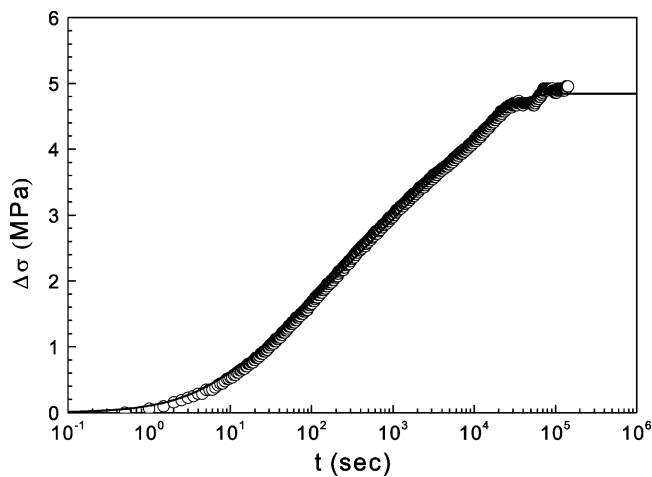


**Figure 14.** Stress relaxation curve from Figure 6 in a comparison with model calculations ( $\tau_r = 1.6 \times 10^4$  s,  $\sigma_0 = 0.55$  MPa,  $\Delta\sigma_r(\infty) = 4.8$  MPa).

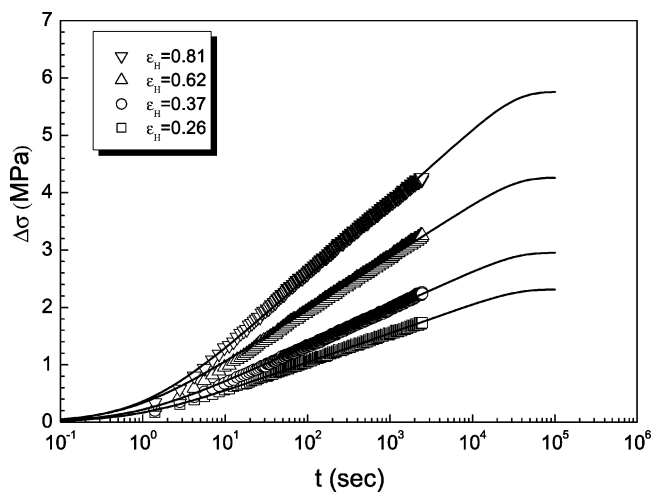


**Figure 15.** Curves from Figure 7 in a comparison with model calculations ( $\tau_r = 1.6 \times 10^4$  s,  $\sigma_0 = 0.22, 0.28, 0.40,$  and  $0.56$  MPa,  $\Delta\sigma_r(\infty) = 2.3, 3.0, 4.2,$  and  $5.7$  MPa).

relaxation, given by  $\sigma_r(0)$ , obviously increase with rising strain. The values  $\sigma_0$  derived from the slopes are shown in Figure 16. Interesting to note in this dependence the critical strains at locations A, B, and C show up again. To represent the observed dependence, we just choose a stepwise linear function, with the first line going from the origin to the value of  $\sigma_0$  at point A, followed by a line going to  $\sigma_0$  at B, a further one continuing to point C, and a final line with a slope according to the experiment. Looking at the data given in the legends also indicates that for the total amount of stress relaxation,  $\Delta\sigma(\infty)$ , a proportionality to  $\sigma_0$  holds

$$\sigma_r(0) = \Delta\sigma(\infty) \sim \sigma_0 \quad (21)$$

The values  $\Delta\sigma(\infty)$  can now be used to derive the quasi-static stress–strain relationship from a stress–strain curve measured at some finite strain rate. The filled symbols presented in Figure 8 were obtained in this manner.

**5.2. Stress Contributions from the Amorphous Network and the Crystal Skeleton.** The model describes the quasi-static stress–strain relationship as originating from two contributions, given by the amorphous network, with a stress  $(1 - \phi_c)\sigma_n$ , and the crystal skeleton, with the stress  $\phi_c\sigma_c$ . A separation of the two

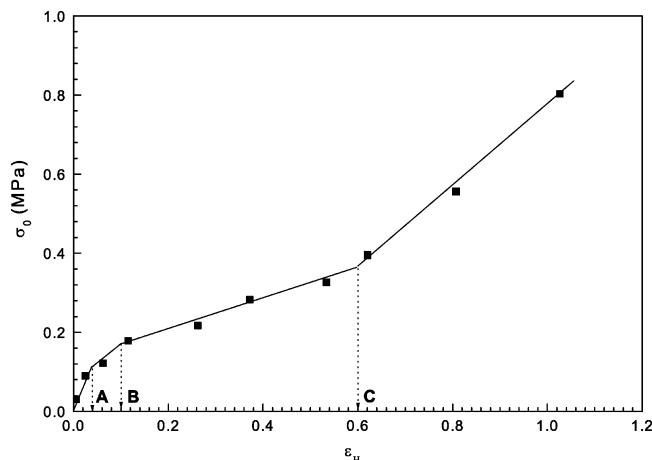


**Figure 16.** Variation of the reference stress  $\sigma_0$  with the imposed strain as derived from the slopes of the stress relaxation curves in Figure 7.  $\sigma_0$  controls the magnitude of stress relaxation. The dependence can be described by a series of lines beginning at the origin with changes at the critical strains A ( $\epsilon_H = 0.04$ ,  $\sigma_0 = 0.11$ ), B ( $\epsilon_H = 0.10$ ,  $\sigma_0 = 0.16$ ), and C ( $\epsilon_H = 0.6$ ,  $\sigma_0 = 0.40$ ).

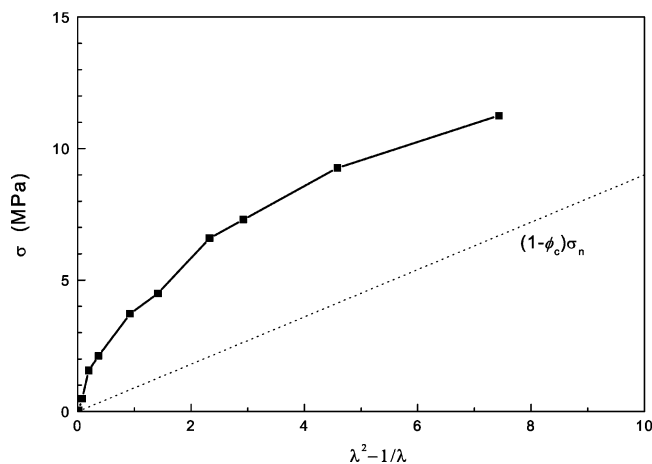


**Figure 17.** Quasi-static stress–strain dependence shown in Figure 8 presented in a plot of  $\sigma$  vs  $\lambda^2 - 1/\lambda$ . The broken line represents a Gaussian network with  $G = 1.3$  MPa.

contributions becomes possible considering that in the limit of high strains the network force becomes dominant. We, therefore, plot as suggested long ago by Haward and Thackray<sup>17</sup> the total quasi-static stress

$$\phi_c \sigma_c + (1 - \phi_c) \sigma_n \quad (\phi_c \text{ denotes the crystallinity})$$

versus  $\lambda^2 - 1/\lambda$ , the measure of strain to be used for an ideal rubber. Figure 17 presents such a plot. The straight line showing up in the asymptotic limit confirms that the assumed dominance of rubber elastic forces at high strains is indeed given. The slope of this line yields the shear modulus of the Gaussian network:

$$(1 - \phi_c) \sigma_n = (1 - \phi_c) G (\lambda^2 - 1/\lambda) \quad (22)$$

The value obtained for this sample is  $G = 1.3$  MPa. This agrees with values given in the literature for the shear modulus of polyethylene, as it follows from either the elastic plateau in the melt determined by dynamic measurements or stress–strain measurements on samples with near-to-zero crystallinity.<sup>18</sup>

The agreement implies that the stress  $\sigma_c$  which is transmitted by the crystal skeleton approaches for high

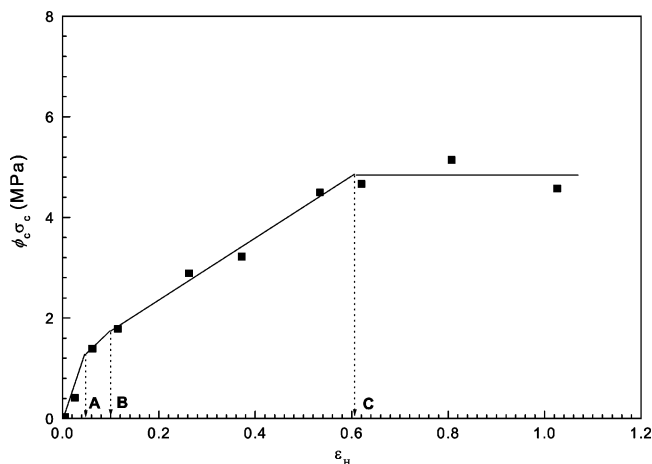


**Figure 18.** Quasi-static stress–strain curve associated with the crystal skeleton, as obtained from the curve in Figure 17 after subtraction of the network stress. Representation by a series of lines with changes at the critical strains A, B, and C.

strains a constant value.  $\sigma_c(\epsilon_H)$  is obtained by a subtraction of the network stress from the total static value, and the result is shown in Figure 18. Interesting to note,  $\sigma_c$  reaches the plateau value at point C after an initial increase. This again indicates that the limitation of the elasticity of drawn samples originates from the crystal skeleton only.

**5.3. Three-Component Representation of the Stretching Curve.** So far we have determined the model parameters related to the stresses contributed by the crystal skeleton and the amorphous network and also two of the three parameters which are included in the relaxing stress component, namely, the strain-dependent reference stress  $\sigma_0(\epsilon_H)$  and the constant final relaxation time  $\tau_r = \eta_0/E_r$ . There remains only one parameter,  $E_r$  or  $\eta_0$ , to be determined. This can be achieved by a final adjustment which should lead to an agreement of the model with the measured stress–strain curve. Given the common development of the strain in all three components of the model and referring to the relaxing stress branch, we write for the strain rate

$$\dot{\epsilon}_H = \frac{\dot{\sigma}_r}{E_r} + \dot{\epsilon}_0 \sinh\left(\frac{\sigma_r}{\sigma_0}\right) \quad (23)$$

$$\dot{\epsilon}_H = \frac{d\sigma_r}{d\epsilon_H} \frac{\dot{\epsilon}_H}{E_r} + \dot{\epsilon}_0 \sinh\left(\frac{\sigma_r}{\sigma_0}\right) \quad (24)$$

Rewriting of the equation yields

$$\frac{d\sigma_r}{d\epsilon_H} = E_r - \frac{\dot{\epsilon}_0 E_r}{\dot{\epsilon}_H} \sinh\left(\frac{\sigma_r}{\sigma_0(\epsilon_H)}\right) = E_r - \frac{\sigma_0(\epsilon_H)}{\tau_r \dot{\epsilon}_H} \sinh\left(\frac{\sigma_r}{\sigma_0(\epsilon_H)}\right) \quad (25)$$

Since

$$\tau_r = \eta_0/E_r$$

is strain-independent, both the viscosity coefficient  $\eta_0$  and the modulus  $E_r$  will also have constant values. Because of the strain dependence of  $\sigma_0$ , this differential equation for  $\sigma_r$  cannot be evaluated analytically but in an easy straightforward way by numerical means. One

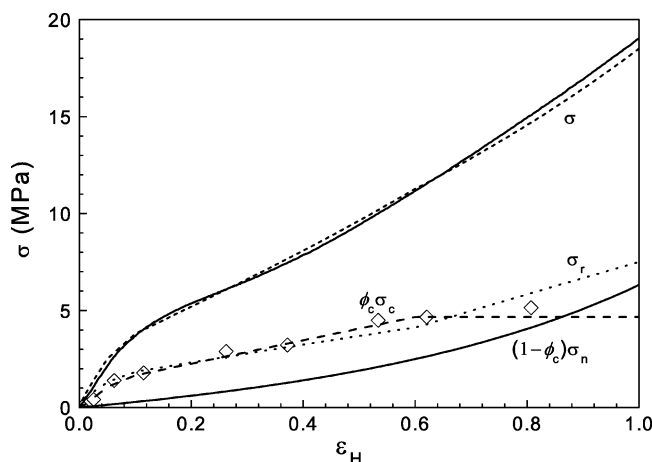


**Figure 19.** Decomposition of the stretching curve shown in Figure 8 in the three components of the model in Figure 12: quasi-static elasto-plastic contribution of the crystal skeleton ( $\phi_c \sigma_c$ ; from Figure 18), elastic stress of the entanglement network ( $(1 - \phi_c) \sigma_n$ ;  $G = 1.3$  MPa), and relaxing viscous stress ( $\sigma_r$ ;  $E_r = 90$  MPa,  $\tau_r = 1.6 \times 10^4$  s,  $\sigma_0$  from Figure 16).

can start at the origin ( $\sigma_r = 0$ ,  $\epsilon_H = 0$ ) and carry out a stepwise integration introducing the regionwise defined function  $\sigma_0(\epsilon_H)$  together with the known value for  $\tau_r$ . The contributions of the two other branches,  $\phi_c \sigma_c$  and  $(1 - \phi_c) \sigma_n$ , are already fixed. The only variable which is unknown is the modulus  $E_r$ . It can be determined by a least-squares fitting procedure, and the result is shown in Figure 19. The figure presents as our final result the decomposition of the total stress in the three parts  $\phi_c \sigma_c$ ,  $(1 - \phi_c) \sigma_n$ , and  $\sigma_r$ , derived for the stretching test carried out with a strain rate  $\dot{\epsilon}_H = 0.005$  s $^{-1}$ . The agreement between the measured and the synthesized curve looks satisfactory and was achieved choosing for the modulus the value  $E_r = 90$  MPa. From  $\tau_r$  and  $E_r$  there follows for the Newtonian viscosity coefficient the result  $\eta_0 = 1.4 \times 10^6$  MPa s. As the analysis shows, skeleton force and viscous stresses from the inception are of similar order. The network stress is at first negligible but finally dominates. The analysis points in particular at a steady increase of the viscous force. This increase is not related to an increasing Newtonian viscosity  $\eta_0$ , which is apparently constant, but is due, formally speaking, to a coupled increase of both Eyring parameters  $\sigma_0$  and  $\dot{\epsilon}_0$ . The reference stress  $\sigma_0$  can be related to an “activation volume”  $v_A$  by

$$\sigma_0 = \frac{kT}{v_A}$$

The observation then means that  $v_A \sim 14$  nm $^3$  for  $\epsilon_H = 0.4$ , which is on the order of the size of the crystal blocks—decreases with increasing strain.

## 6. Conclusion

Experiments probing uniaxial tensile deformation of semicrystalline polymers indicate (1) a finite amount of stress relaxation in drawn samples leading into a quasi-stationary state, (2) a finite amount of plastic flow for any imposed strain, again leading into a quasi-stationary state, (3) a homogeneous strain distribution in stretched samples, and (4) the presence of viscous forces which obey Eyring’s law. On the basis of these observations, a model is constructed composed of three branches with a common strain. Two branches, with stresses  $\phi_c \sigma_c$  and  $(1 - \phi_c) \sigma_n$ , relate to the quasi-stationary state of the skeleton of crystallites and the amorphous network; the third branch dealing with the relaxing stress  $\sigma_r$  accounts in a global manner for all viscous forces which become effective for nonzero strain rates. Details of the kinetics of stress relaxation can be reproduced. Application of the model, demonstrated for a comprehensive set of data obtained for a poly(ethylene-co-vinyl acetate), yields a decomposition of measured stresses in the viscous part and the quasi-static contributions of the network and the crystalline skeleton.

**Acknowledgment.** Support of this work by the Deutsche Forschungsgemeinschaft (Sonderforschungsbereich 428) is gratefully acknowledged. Thanks are also due to the Fonds der Chemischen Industrie for financial help. We greatly appreciate the advice in numerical works given by Werner Stille.

## References and Notes

- (1) Hiss, R.; Hobeika, S.; Lynn, C.; Strobl, G. *Macromolecules* **1999**, *32*, 4390.
- (2) Al-Hussein, M.; Strobl, G. *Macromolecules* **2002**, *35*, 8515.
- (3) Men, Y.; Strobl, G. *J. Macromol. Sci., Phys.* **2001**, *B40*, 775.
- (4) Men, Y.; Strobl, G. *Macromolecules* **2003**, *36*, 1889.
- (5) Hobeika, S.; Men, Y.; Strobl, G. *Macromolecules* **2000**, *33*, 1827.
- (6) Yang, Y. C.; Geil, P. H. *Makromol. Chem.* **1985**, *186*, 1961.
- (7) Hugel, T.; Strobl, G.; Thomann, R. *Acta Polym.* **1999**, *50*, 214.
- (8) Godehardt, R.; Rudolph, S.; Lebek, W.; Goerlitz, S.; Adhikari, R.; Allert, E.; Giesemann, J.; Michler, G. H. *J. Macromol. Sci., Phys.* **1999**, *B38*, 817.
- (9) Al-Hussein, M.; Strobl, G. *J. Polym. Sci., Phys. Ed.* **2004**, *42*, 2074.
- (10) Boyce, M. C.; Socrate, S.; Llana, P. G. *Polymer* **2000**, *41*, 2183.
- (11) Dieter, G. E. *Mechanical Metallurgy*; McGraw-Hill: New York, 1986; p 432.
- (12) Bergstrom, J. S.; Boyce, M. C. *J. Mech. Phys. Solids* **1998**, *46*, 931.
- (13) Buckley, P. C.; Jones, D. C. *Polymer* **1995**, *37*, 2403.
- (14) Argon, A. S. *Philos. Mag.* **1973**, *28*, 839.
- (15) Tervoort, T. A.; Klompen, E. T. J.; Govaert, L. E. *J. Rheol.* **1996**, *40*, 779.
- (16) Govaert, L. E.; Timmermans, P. H. M.; Brekelmans, W. A. M. *J. Eng. Mater. Technol.* **2000**, *122*, 177.
- (17) Haward, R. N.; Thackray, G. *Proc. R. Soc. London A* **1968**, *302*, 453.
- (18) Krigas, T. M.; Carella, J. M.; Struglinski, M. J.; Crist, B.; Graessley, W. W.; Schilling, F. C. *J. Polym. Sci.* **1985**, *23*, 509.

MA049174H